FULL PAPER

Flexible Electronics

**ADVANCED
FUNCTIONAL
MATERIALS**

www.afm-journal.de

Piezo-Phototronic Effect for Enhanced Flexible MoS$_2$/WSe$_2$ van der Waals Photodiodes

Pei Lin, Laipan Zhu, Ding Li, Liang Xu, Caofeng Pan,* and Zhonglin Wang*

The recent discoveries of transition-metal dichalcogenides (TMDs) as novel 2D electronic materials hold great promise to a rich variety of artificial van der Waals (vdWs) heterojunctions and superlattices. Moreover, most of the monolayer TMDs become intrinsically piezoelectric due to the lack of structural centrosymmetry, which offers them a new degree of freedom to interact with external mechanical stimuli. Here, fabrication of flexible vdWs p–n diode by vertically stacking monolayer n-MoS$_2$ and a few-layer p-WSe$_2$ is achieved. Electrical measurement of the junction reveals excellent current rectification behavior with an ideality factor of 1.68 and photovoltaic response is realized. Performance modulation of the photodiode via piezo-phototronic effect is also demonstrated. The optimized photoresponsivity increases by 86% when introducing a −0.62% compressive strain along MoS$_2$ armchair direction, which originates from realigned energy-band profile at MoS$_2$/WSe$_2$ interface under strain-induced piezoelectric polarization charges. This new coupling mode among piezoelectricity, semiconducting, and optical properties in 2D materials provides a new route to strain-tunable vdWs heterojunctions and may enable the development of novel ultrathin optoelectronics.

1. Introduction

The emergence of transition-metal dichalcogenides (TMDs) as novel 2D materials beyond graphene has attracted extensive attention from the aspect of fundamental physics study and potential applications in ultrathin devices.[1] The unique morphology and electronic structure give them a variety of intriguing properties that are unattainable in conventional bulk materials.[2] Moreover, unlike the semimetal graphene, the availability of semiconductor TMDs with different bandgaps and work functions enables the fabrication of artificial van der Waals (vdWs) heterojunctions or super-lattices with varying functionalities.[3] Among these 2D vdWs structures, the p–n junction is of special interest as it provides the basic building block for numerous modern electronics and optoelectronics involving photodetectors, light-emitting diodes, ultrafast lasers, and solar cells.[4] In addition to their distinct optoelectronic properties, the atomically thin TMDs also possess superior mechanical properties that far excel bulk and even some 1D nanowires. It is reported that the monolayer MoS$_2$ has the ability to withstand 11% strain before fracture, rendering it a promising candidate for wearable electronics, nanorobotics, and human–machine interfacing applications.[5]

Mechanical strain is ubiquitous and exists throughout the whole process from material synthesis, device fabrication to their final service condition. How to deal with the strain remains an outstanding challenge for the 2D materials before their practical applications. Although several 2D TMD-based flexible devices have been reported, normally constant performance under the action of external strain are expected.[6] However, the emerging applications in wearable and smart electronics also require active interactions between the devices and environment strain stimuli, which means that the functional electronics or optoelectronics can be directly modulated by mechanical agitations. Piezoelectric materials, which have been historically used in electromechanical coupling applications, could act as an enabler for such requirement. Recently, numerical calculations and experimental results demonstrated that many of the atomically thin TMDs at the center of current research focus are intrinsically piezoelectric due to the lack of inversion symmetry.[7] And most of them such as MoS$_2$ and MoTe$_2$ have predicted or measured piezoelectric coefficients comparable to standard bulk piezoelectric ZnO and AlN crystals,[8] making them the materials of choice for thinnest actuators and nanogenerators. In addition, unlike the conventional insulating lead zirconate titanate (Pb(Zr$_x$Ti$_{1−x}$)O$_3$, PZT), semiconducting 2D TMDs offer another coupling mode among piezoelectricity, semiconducting, and optical properties in them, which is the piezo-phototronic effect. It refers to the use of strain-induced piezoelectric-polarization to regulate the generation, transport, separation, and/or the recombination process of photoexcited carriers at Schottky or p–n junction interface for optoelectronics

Dr. P. Lin, Dr. L. Zhu, Dr. D. Li, Dr. L. Xu, Prof. C. Pan, Prof. Z. L. Wang
CAS Center for Excellence in Nanoscience
Beijing Key Laboratory of Micro-nano Energy and Sensor
Beijing Institute of Nanoenergy and Nanosystems
Chinese Academy of Sciences
Beijing 100083, P. R. China
E-mail: cfpan@binn.cas.cn; zhong.wang@mse.gatech.edu
Dr. P. Lin, Dr. L. Zhu, Dr. D. Li, Dr. L. Xu, Prof. C. Pan, Prof. Z. L. Wang
School of Nanoscience and Technology
University of Chinese Academy of Sciences
Beijing 100049, P. R. China
Prof. Z. L. Wang
School of Material Science and Engineering
Georgia Institute of Technology
Atlanta, GA 30332, USA

The ORCID identification number(s) for the author(s) of this article can be found under https://doi.org/10.1002/adfm.201802849.
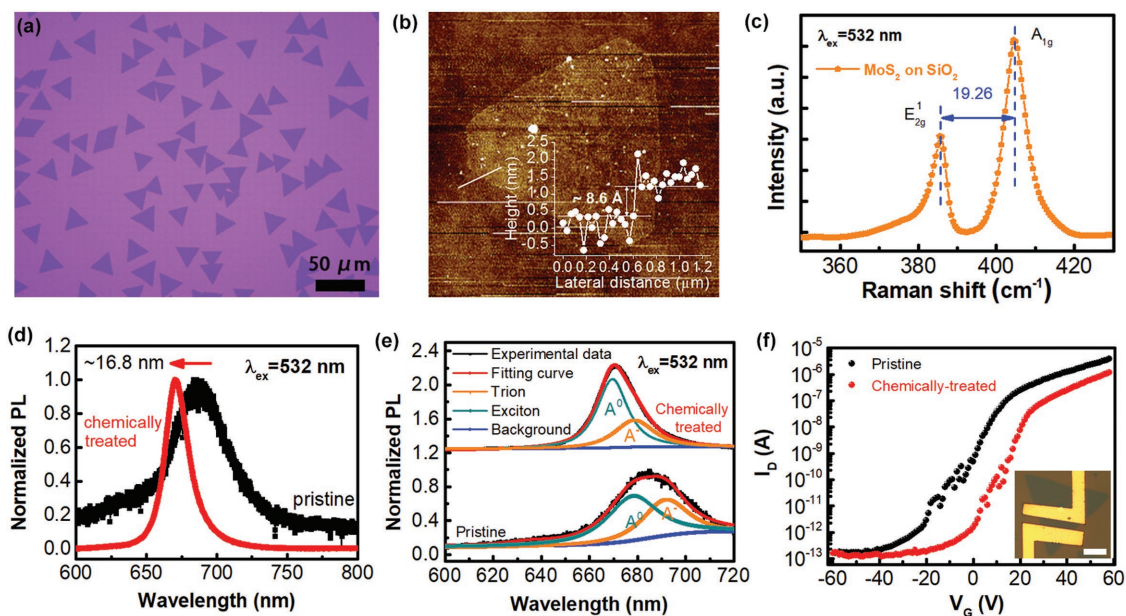
1802849 (1 of 8)

Figure 1. a) Optical image of the synthetic MoS_2 on SiO_2/Si substrate. b) AFM image of MoS_2 flake. Inset: cross-sectional profile along the white line. c) Typical Raman spectrum of the MoS_2 flakes. d) Normalized PL spectrum for both as-synthesized and TFSI-treated MoS_2 monolayer. e) Curve-fitting analysis of the PL spectra in panel (d). The A peaks were reproduced by assuming trion (A^-) and exciton (A^0) peaks with Lorentzian functions. f) Transfer characteristics of the monolayer MoS_2 before and after TFSI treatment. Inset shows optical image of the fabricated FET, scale bar is 10 μm.

performance modulation.[9] This effect has been successfully demonstrated in wurtzite ZnO and GaN optoelectronics such as light-emitting diode, solar cells, and photosensors.[10] Precise tunability over junction property is critical to the operation of functional vdWs electronics/optoelectronics. Until now, most of the reported manipulation of 2D vdWs p–n junction was achieved by electrostatic gating on hard substrates.[11] However, direct implementation of the junction control with external strain stimuli can be more attractive, which may simplify the flexible device structure and facilitate a higher level of system integration.

In this study, we developed a flexible vdWs heterojunction photodiode on polyethylene terephthalate (PET) substrate using synthetic monolayer n-MoS_2 and multilayer p-WSe_2. The strain-gated photoresponse was achieved and piezo-phototronic effect was demonstrated to dominate the performance modulation. When specific strain was applied, the piezoelectric polarization charges in monolayer MoS_2 adjusted the local band profile tilting at heterojunction interface. The realigned energy band promoted separation of photogenerated electron–hole pairs more effectively, and enhanced their transport and extraction to contacts. The optimized photoresponsivity increased by 86% while introducing a –0.62% compressive strain along the MoS_2 armchair direction. Our results demonstrate the feasibility of using piezo-phototronic effect to realize strain-tunable vdWs heterojunctions, which may offer a new approach to implement high-performance flexible TMDs optoelectronics and enable the development of novel ultrathin devices.

2. Results and Discussion

Both MoS_2 and WSe_2 flakes used in the experiment were synthesized on SiO_2/Si via chemical vapor deposition (CVD)

approach (Note 1, Supporting Information).[12] The morphology of as-grown MoS_2 crystal was investigated by optical microscope, where the MoS_2 exhibits typical triangular shape with the length of triangle side ≈40 μm, as shown in **Figure 1**a. Figure 1b displays the atomic force microscopy (AFM) image of MoS_2 flake, which demonstrates its smooth surface topography and thickness was measured to be ≈0.86 nm. Two characteristic peaks of in-plane E^1_{2g} and out-of-plane A_{1g} vibration modes were observed in the Raman spectrum, with their frequency separation ≈19.3 cm^{-1}, as presented in Figure 1c. As it is well known, the E^1_{2g} mode softens and A_{1g} stiffens with increasing MoS_2 thickness, their peak position difference could be used as an indicator of the layer number.[13] From Raman and AFM characterization results, it can be confirmed that the CVD MoS_2 flake is monolayer. Compared with the bulk stacked-layer MoS_2 crystal, this atomically thin MoS_2 film is intrinsically piezoelectric due to the lack of inversion symmetry. Since the CVD-synthesized 2D materials were demonstrated to be host to a wide range of defect types, several defects engineering approaches have been proposed to improve the materials' quality.[14] Here, bis(trifluoromethane)sulfonamide (TFSI) treatment for the as-synthesized MoS_2 was performed before devices fabrication process (details in Experimental Section).[15] As shown in Figure S1 (Supporting Information), with the increase of TFSI treatment time, MoS_2 photoluminescence (PL) intensity increases significantly and the photon energy blue shifts. After 15 min treatment, optimized PL intensities reach the maximum with a ≈20-fold enhancement over the pristine ones and peak position blue shifts by 16.8 nm (Figure 1d). Meanwhile, the full width at half-maximum (FWHM) of PL peaks reduce from 43.6 to 18.7 nm. Although the exact mechanism of defects passivation via TFSI was not fully understood, reduction of sulfur vacancies through rearrangement of surface
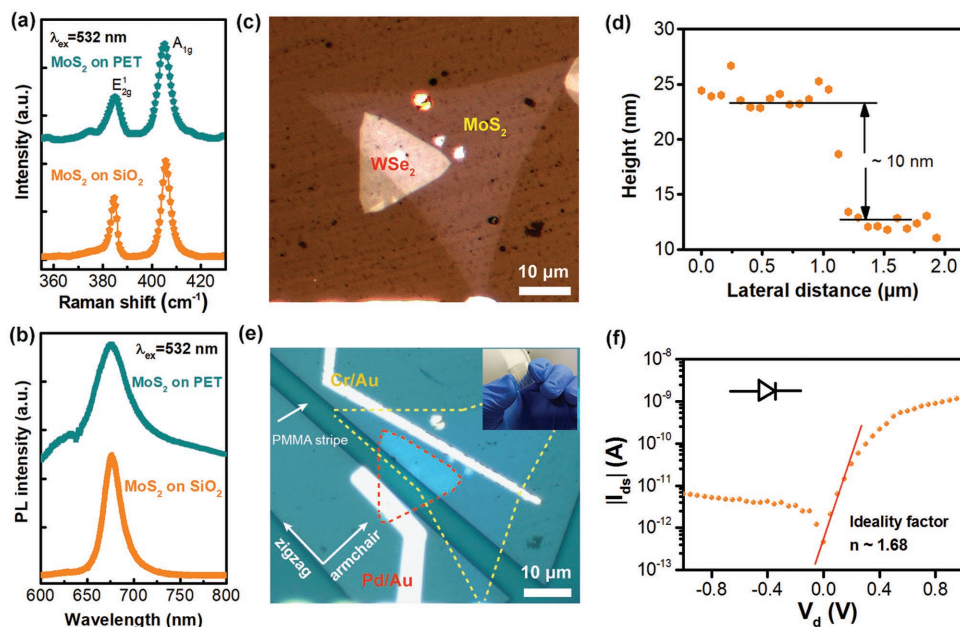
**ADVANCED
SCIENCE NEWS**

www.advancedsciencenews.com

**ADVANCED
FUNCTIONAL
MATERIALS**

www.afm-journal.de

Figure 2. Comparison of a) Raman and b) PL spectra of MoS_2 on SiO_2/Si and MoS_2 after transfer onto PET. c) Optical microscopy image of MoS_2/ WSe_2 heterostructure stack on PET substrate. d) AFM line profile of the WSe_2 flake shows its thickness of ≈10 nm e) Optical image of the fabricated MoS_2/ WSe_2 p–n photodiode device. f) Current-voltage curve of the flexible p–n diode in logarithmic scale.

sulfur adatoms was considered as one possibility. In addition, these PL features are consistent with previous theoretical study that with the increasing charge states of vacancies, the monolayer MoS_2 bandgaps get smaller.[16] To further reveal these spectral change, curve fitting result of PL peak A is shown in Figure 1e by considering the contribution of exciton (A^0) and trion (A^-). It can be seen that the spectral weight of negative trion peak becomes much smaller after TFSI treatment, which indicates the decrease of excess carrier density in MoS_2.[14b,17] Another evidence for this comes from the field-effect transistor characterization, a clear right-shifting of threshold voltage for the treated MoS_2 transistor was observed in the transfer characteristic curves (Figure 1f). The reduction of defects and free carrier concentration would weaken the screening effect in piezoelectric monolayer MoS_2, which is beneficial for the following piezo-phototronic modulation of devices performance.

The PL and Raman properties of MoS_2 were monitored at each step during the device assembly process, as shown in **Figure 2**a,b. Here, the PET was selected as flexible substrate due to its good solvent-resistant property and relatively high Young's modulus, which ensures that the substrate-induced strain can be effectively transferred to MoS_2.[18] It can be seen that both of the frequency separation in Raman spectra and PL peak position are well preserved except a slight broadening for FWHM of PL peak, which suggests no obvious performance degradation after its transfer onto PET. The optical microscope image of a typical MoS_2/WSe_2 stack on PET substrate is shown in Figure 2c. The multilayer WSe_2 film was identified by using Raman spectroscope (Figure S2, Supporting Information) and its thickness was estimated to be ≈10 nm from the AFM result, as shown in Figure 2d. Because of the anisotropic piezoresponse in monolayer MoS_2, the applied strain in our experiment is in parallel to armchair direction of triangular MoS_2, along which

it possesses the most significant piezoelectric effect and largest piezoelectric coefficient.[19] Moreover, previous studies indicate that two dominant morphologies exist in CVD MoS_2, and the molybdenum zigzag triangles have straighter and sharper edge than sulfur zigzag triangles.[20] Figure 2e displays the optical image of fabricated MoS_2/WSe_2 p–n diode device on PET. From the optical morphology, it can be speculated that MoS_2 with sulfur zigzag triangles was used in our devices. Electrical measurement of the p–n junction under dark and strain-free condition is shown in Figure 2f, which reveals excellent current rectification behavior with an ideality factor of 1.68. The ON/ OFF ratio is about 202 under ±1 V operating voltage.

Figure 3a shows J–V curves of the flexible diode upon 532 nm laser illumination with incident power from 0.57 to 6.67 mW cm^{-2}. The illumination intensity was elaborately controlled to avoid polymer substrate heating and eliminate the influence of photothermoelectric effect (Figure S3, Supporting Information). From J–V characteristics, it is observed that the diode shows an obvious photovoltaic response. Therefore, this device can be operated as a photodiode under zero bias mode to maximize the signal-to-noise ratio. The short-circuit current J_{sc} and open-circuit voltage V_{oc} as a function of illumination power density P_i were presented in Figure 3b,c. The J_{sc} shows linear dependency with P_i and no saturation was observed in the measured range. Because of the negligible dark current at zero bias, photoresponsivity of the diode reaches ≈1.8 mA W^{-1} under photovoltaic mode for different P_i, which is defined as $R = I_{ph}/P_i$, where I_{ph} is the photocurrent density. Such constant photoresponsivity independent on incident optical power is critical for many practical applications. The V_{oc} also scales with the P_i, which is consistent with the conventional p–n junction theory. However, the measured value is lower than the theoretical maximum; low incident optical power may be one of the
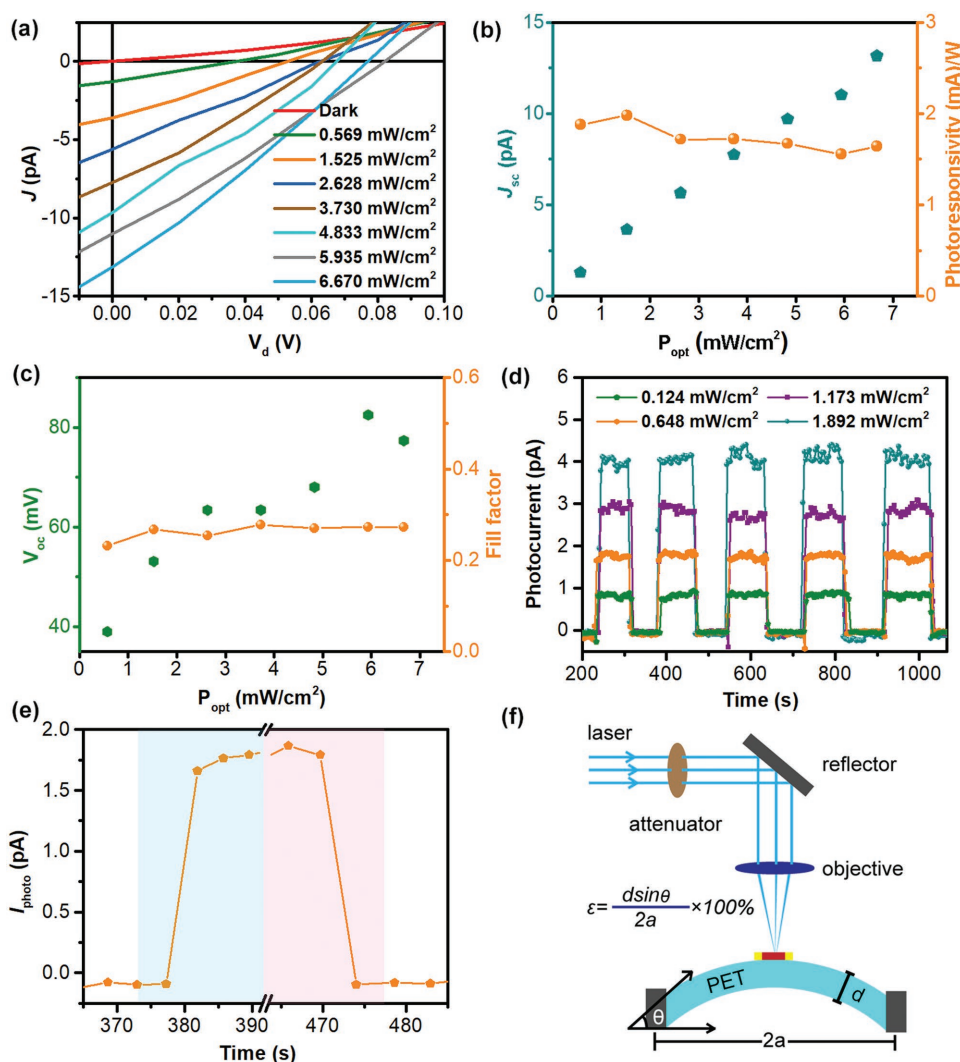
Figure 3. a) J–V characteristics of the device under dark and different 532 nm optical illumination intensities. b) Short-circuit current J_{sc}, photoresponsivity and c) open-circuit voltage V_{oc}, fill factor as a function of optical power with the data extracted from panel (a). d) Temporal response of the photocurrent generation under optical illumination at zero bias. e) Response time of the device, with the data extracted from (d). f) Schematic of experimental setup for characterizing piezo-phototronic process in the fabricated heterojunction device.

major reasons responsible for this. Besides, electrical transport properties of MoS_2 and WSe_2 might get worse on the polymer substrate and the large series resistance could also reduce V_{oc}. Moreover, the large channel width may increase the recombination probability of photoexcited electron–hole pairs, also making the V_{oc} smaller than theoretical value. Therefore, it is speculated that performance of such flexible vdWs photovoltaics can be further enhanced through optimizing the devices geometry. The fill factor is ≈0.28 and shows little variations with illumination power. The photo-switching characteristic and stability of the flexible photodiode were investigated at room temperature in air, as shown in Figure 3d. The photocurrent increases rapidly to ON state (pA range) under illumination and can keep constant for >100 s, then it resumes to OFF state (several fA range) under dark, an obvious switching behavior is observed. Figure 3e shows the corresponding response time of the device. Here, response time of the temporal photoswitching may not be accurately determined, as it is beyond the time

resolution of Keithley 4200 and a much faster response time could be expected. Besides, this ON/OFF property could be well retained after several cycling tests in ≈800 s, demonstrating good stability and repeatability of the device under various illumination conditions. Schematic of the home-made setup for characterizing the piezo-phototronic process in the devices is shown in Figure 3f (details in Experimental Section; Note 2 and Figure S4, Supporting Information). The uniaxial tensile and compressive strain could be achieved through bending flexible substrate upward and downward, respectively, with their magnitude proportional to bending curvature and being controlled through manipulation of bending separation.

Before characterizing the changes in MoS_2/WSe_2 photodetection performance with strain, electrical transport of the flexible diode under mechanical strain without optical illumination was firstly measured, as shown in **Figure 4**a. An obvious strain-gated vdWs junction property was demonstrated. The turn-on voltage of diode was effectively tuned, current in forward bias
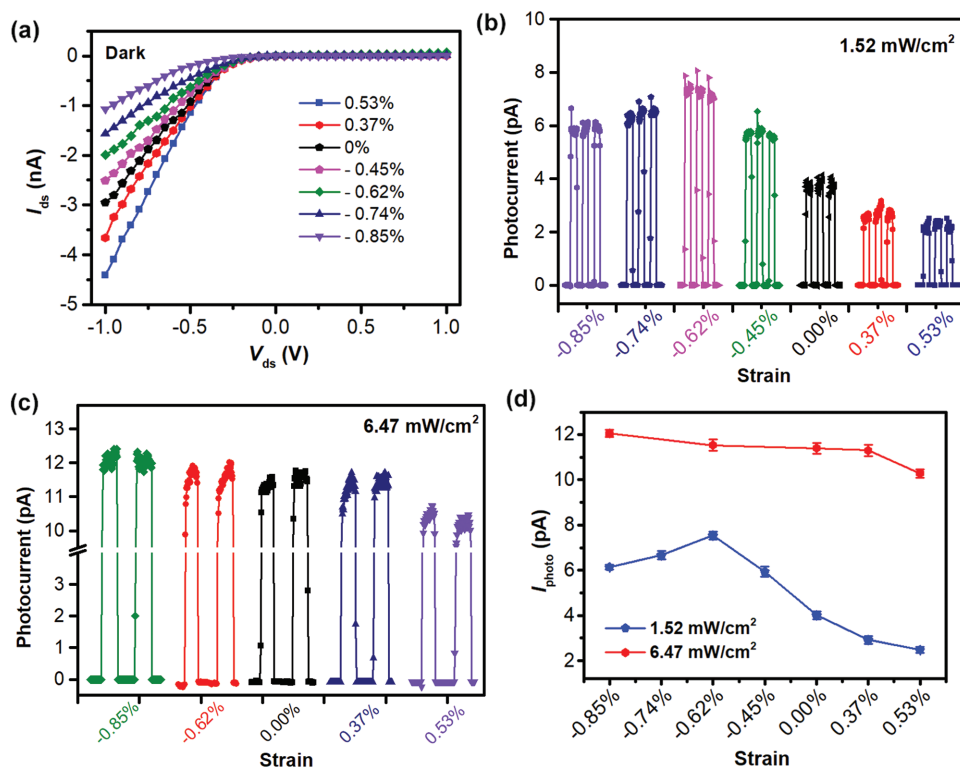
Figure 4. Piezo-phototronic characterization in the flexible MoS_2/WSe_2 p–n photodiode. a) Typical electrical transport of the vdWs heterojunction in dark under various strains. Strain dependence of photocurrent in the device under the illumination of b) 1.52 mW cm^{-2} and c) 6.47 mW cm^{-2} light at zero applied bias. d) Calculated photocurrent as a function of applied strain for different illumination intensity.

decreases with increasing compressive strain and increases with tensile strain. Here, two effects may give rise to the observed transport change in our devices: piezoresistive effect, which means a change in electrical resistivity due to the change in band structure and density of states of carrier when mechanical strain is applied; the other is piezotronic effect, where strain-induced piezopolarization charges function as "gate" voltage to tune interface barrier height and the carrier transport properties. Under zero bias and 532 nm optical illumination, the mechanical strain could further modulate the photodiode response. At low optical power density of 1.52 mW cm^{-2}, the photocurrent decreases with tensile strain, while the photocurrent firstly increases and then decreases with the further increase of applied compressive strain (Figure 4b). The photocurrent shows the greatest increase by 86% under −0.62% static strain, reaching a maximum photoresponsivity of ≈3.4 mA W^{-1}. The modulation effect of strain for devices under higher illumination density of 6.47 mW cm^{-2} is shown in Figure 4c, only a photocurrent increase of 6.1% was achieved and no turning point was observed in the whole range of applied strain. This suggests that modulation impact of mechanical strain on device performance is optical power-dependent and the effect attenuate seriously with the increase of detected light intensity, as presented in Figure 4d. This phenomenon rules out the possible underlying mechanism that photoresponse modulation originates from strain-induced light absorption change in materials and the piezoresistive effect. Moreover, both previous theoretical calculation and experimental results indicate that

variations in MoS_2 and WSe_2 absorption spectra under strain are rather small, which is not consistent with the measured large photocurrent change.[21] Therefore, it can be speculated that in our devices, the strain-induced changes of electrical transport and photoresponse behavior mainly come from the influence of piezo-phototronic effect, which is to use the piezopotential to modulate the carrier generation, transport, separation, and/or recombination process at the interface for optoelectronics performance control.

To further elucidate the modulation mechanism of piezo-phototronic effect, energy band diagrams are introduced to understand the observed phenomena. **Figure 5**a shows the schematic band profile of MoS_2/WSe_2 p–n heterojunction under strain-free and zero bias condition. Taking into account the difference in work function and bandgap between these two materials, a type II band alignment was predicted,[22,4a] which is consistent with the diode-like transport characteristic. As the 532 nm visible light penetration depth is larger than the junction thickness, photons are absorbed in both MoS_2 and WSe_2 upon the optical illumination, resulting in the photoexcited electron–hole pairs in both materials. However, we can speculate that WSe_2 should dominate the whole light absorption because light was illuminated from WSe_2 side and it is much thicker than monolayer MoS_2. Spontaneous dissociation of photogenerated excitons into free carriers can be actuated by the built-in potential in the overlapped junction region, driving the electrons (holes) to MoS_2 (WSe_2). These free carriers then diffuse laterally to the contact and give rise to the photocurrent. No measurable
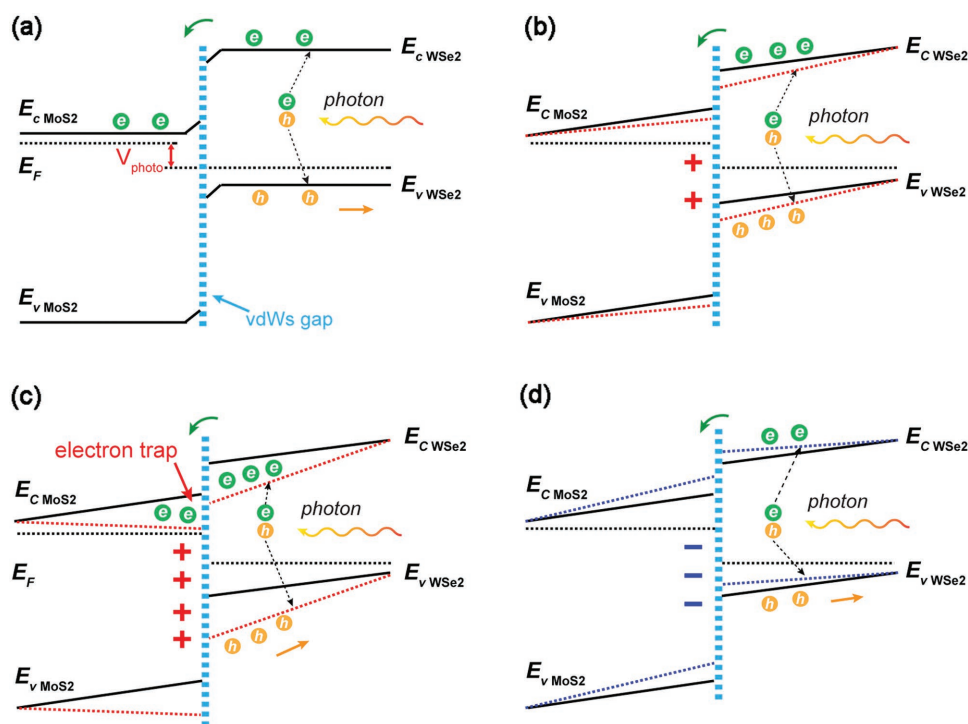
Figure 5. Working mechanism of the piezo-phototronic effect in MoS_2/WSe_2 flexible photodiode. a) Schematic illustration of monolayer n-MoS_2/few-layer p-WSe_2 band diagram and the photovoltaic effect under strain-free and zero bias condition. b) Energy-band profile change in the junction area when moderate positive piezopolarization charges are induced in MoS_2. c) Modulation effect of larger density positive piezocharges on the heterojunction interface, which shows the formation of electron traps. d) Effect of negative piezopolarization charges on the junction band profile.

photocurrent was expected from the carriers outside p–n junction regions because of their low spontaneous separating efficiency under zero bias.[4a] Therefore, the photocurrent is mainly affected by the junction barrier property and largely depends on the effective separation and transport process of carriers at the vicinity of the interface. With external mechanical strain applied on the device, piezoelectric polarization charges are generated at the monolayer MoS_2 zigzag edge because of its lack of centrosymmetry, while the piezoresponse in thick WSe_2 layers can be ignored.[7c] The interface band structure and thus the carriers' behavior could be directly affected by these strain-induced piezoelectric charges, which have been confirmed theoretically and experimentally in MoS_2/Pd Schottky contact.[21a,23] Due to the ultrathin nature of 2D semiconductors, there would be no significant band-bending at the junction interface but forming a monotonic band slope in each material.[4a,11a,24] Considering the crystal orientation of used triangular MoS_2, positive piezopolarization charges are created at the MoS_2/WSe_2 p–n junction contact when applying compressive strain. Realignment of the interface band tilting is shown in Figure 5b, the band slope in MoS_2 becomes gentle while a steeper band slope is formed in WSe_2 under the action of these positive piezoelectric charges. For the requirement of system charge neutrality, the change of "depletion width" in each side could be calculated as (Note 3 and Figure S5, Supporting Information):

$$\Delta L_{MoS_2} = -\frac{\varepsilon_1 Q_{piezo}}{\varepsilon_1 N_D + \varepsilon_2 N_A} \tag{1}$$

$$\Delta L_{WSe_2} = \frac{\varepsilon_2 Q_{piezo}}{\varepsilon_1 N_D + \varepsilon_2 N_A} \tag{2}$$

where ε_1, N_D is the dielectric constant and concentration of donors in MoS_2; ε_2, N_A is the dielectric constant and concentration of acceptors in WSe_2. Q_{piezo} is the piezoelectric polarization charges. Due to the larger dielectric constant of multilayer WSe_2 than the monolayer MoS_2, the strength of built-in potential was enhanced under compressive strain at the beginning, which is in agreement with the electrical measurements in Figure 4a. This means that these positive piezocharges function as applied reverse bias, providing extra driving force for the rapid separation of photoinduced excitons. As a consequence, the injection of photoexcited electrons in WSe_2 into MoS_2 could be promoted more effectively, as well as their transport and extraction to the electrodes. Therefore, the interlayer recombination of electron–hole at the interface is suppressed and photocurrent firstly increase with the increasing compressive strain.

With the increase of positive polarization charges density at the interface with a further increase of compressive strain, the inclination direction of monotonic band in MoS_2 at the junction would reverse that local trapping effect becomes appreciable at the interface, as shown in Figure 5c. The existence of such strain-induced traps has been verified by theoretical simulation.[9b] Therefore photogenerated electrons will accumulate in this trap and the interlayer electron–hole recombination probability at the junction is increased, leading to reduced rate of collection

of photogenerated carriers and photocurrent decrease under larger compressive strains.

On the contrary, when a tensile strain is introduced, induced negative piezopolarization charges in MoS_2 attract holes from WSe_2 and decrease the built-in potential in it, which decreases the driving force for excitions dissociation (Figure 5d). Besides, these negative charges repel photogenerated electrons in WSe_2, reducing their injection efficiency into MoS_2. Therefore, decreased photocurrent was observed under the tensile strains. In addition, at high illumination intensity, the carrier concentration N_D and N_A in MoS_2 and WSe_2 increases, so the screening effect of piezoelectric polarization charges are enhanced, resulting in lower density of effective Q_{piezo}.[25] From Equations (1) and (2), it can be seen that the modulation impact of strain on photocurrent should be more significant under low optical intensity, which is consistent with the results in Figure 4b,c. As the piezocharges can be generated both at MoS_2/WSe_2 and MoS_2/Cr contacts when applying mechanical strain, the influence of piezo-phototronic effect on the MoS_2/Cr interface should also be taken into account. Considering the crystal orientation of MoS_2, it can be speculated that negative piezocharges are created at MoS_2/Cr interface under compressive strain. In this case, the barrier height for electrons in MoS_2 injection into Cr electrode would be increased, leading to reduced carriers collection efficiency and photocurrent. This hypothesis is contrary to the measured results in Figure 4, which indicates that strain-modulation of MoS_2/WSe_2 junction property should dominate the whole performance change. In short, these above results indicate that mechanical strain is able to function as another degree of freedom in this flexible MoS_2/WSe_2 vdWs heterojunction to effectively modulate the optoelectronic performance. Meanwhile, the piezo-phototronic effect which controls interface carrier behavior through strain-induced piezocharges gives rise to the observed photoresponse change.

3. Conclusion

In summary, we have fabricated the flexible MoS_2/WSe_2 vdWs photodiode on PET substrate. The piezo-phototronic effect in such 2D p–n heterojunction and its application in strain-tunable photodetection performance was also studied. Controllable modulation of photoresponse was achieved; the optimized photoresponsivity increases by 86% when introducing a −0.62% compressive strain along MoS_2 armchair direction. This enhancement originates from the modulation of local interface band tilting by strain-induced polarization charges, which facilitate the effective separation and transport of photoexcited carriers. Considering the fact that most of the atomically thin TMDs are intrinsically piezoelectric, the electromechanical coupling in these materials offers another way to interact with external mechanical stimuli. It is expected that the approach in this study might be extended to other artificial vdWs structures or superlattices, which may implement the high-performance flexible 2D optoelectronics and enable the development of other novel ultrathin devices.

4. Experimental Section

Chemically Treated MoS_2 and Devices Fabrication: Chemical treatment of MoS_2 flakes was performed as follows. Firstly, TFSI solution (0.35 mg mL^{-1}) was prepared by dissolving TFSI (35 mg) in 1,2-dichloroethane (100 mL). The SiO_2/Si substrate with MoS_2 flakes was then immersed into the solution and kept on 100 °C hotplate for 15 min. Finally, the sample was blow dried with N_2 and annealed at 100 °C for another 5 min. Fabrication of the flexible MoS_2/WSe_2 heterojunction starts with transfer of the chemically treated monolayer MoS_2 onto PET substrate using polymethyl methacrylate–assisted transfer technique. Few-layer WSe_2 flakes were subsequently transferred onto MoS_2 with the same procedure to form vertically stacked heterojunction. The overlapped MoS_2/WSe_2 samples were selected for the following devices fabrication process. Electrical contacts were patterned with electron beam lithography (EBL) followed by electron beam deposition of Cr/Au (15 nm/50 nm) as Ohmic electrode for MoS_2 monolayer, and Pd/Au (15 nm/50 nm) layer for the WSe_2 to minimize contact resistance. Acetone was used for the lift-off process. To avoid materials slippage when applying strain, a PMMA stripe was prepared using EBL method in the junction area to fix the contact.

Materials Characterization: Surface morphology of the synthetic MoS_2 and WSe_2 flakes on SiO_2/Si and flexible PET substrate were characterized with optical microscope (Zeiss, Axio Imager). The atomic force microscope (Bruker Dimension Icon) was employed to measure the thickness of materials. The quality of MoS_2 and WSe_2 layers were inspected by Raman spectroscopy and photoluminescence (Horiba LabRAM HR Evolution), with an excitation of 532 nm laser. During characterization, laser power was kept below 500 µW to avoid the sample heating effect.

Performance Assessment and Piezo-phototronic Process Test: All of the electrical characterization was performed at room temperature using Keithley 4200-SCS in shielded probe station. The 532 nm laser with tunable power was used as illumination source for the MoS_2/WSe_2 heterojunction photovoltaic and photosensing measurement. A home-made setup was prepared to study the piezo-phototronic process in devices, by measuring the photoresponse under specific mechanical strain and optical illumination power. The strain on MoS_2 was introduced through a two-point bending apparatus. The bent PET substrate was considered as a circular arc for computing the applied strain. Here, negative sign is for compressive strain and positive sign is for the tensile strain. To avoid the sample slippage, direct–indirect bandgap transition of WSe_2 and plastic deformation of PET substrate, the applied strain was relatively small (<1%).

Supporting Information

Supporting Information is available from the Wiley Online Library or from the author.

Conflict of Interest

The authors declare no conflict of interest.

**ADVANCED
SCIENCE NEWS**
www.advancedsciencenews.com

**ADVANCED
FUNCTIONAL
MATERIALS**
www.afm-journal.de

Keywords

[1] a) S. Das, J. A. Robinson, M. Dubey, H. Terrones, M. Terrones, *Annu. Rev. Mater. Res.* **2015**, *45*, 1; b) B. Radisavljevic, A. Radenovic, J. Brivio, V. Giacometti, A. Kis, *Nat. Nanotechnol.* **2011**, *6*, 147; c) Q. H. Wang, K. Kalantar-Zadeh, A. Kis, J. N. Coleman, M. S. Strano, *Nat. Nanotechnol.* **2012**, *7*, 699; d) J. S. Ross, P. Klement, A. M. Jones, N. J. Ghimire, J. Yan, D. G. Mandrus, T. Taniguchi, K. Watanabe, K. Kitamura, W. Yao, D. H. Cobden, X. Xu, *Nat. Nanotechnol.* **2014**, *9*, 268; e) A. Pospischil, M. M. Furchi, T. Mueller, *Nat. Nanotechnol.* **2014**, *9*, 257.

[2] a) A. Splendiani, L. Sun, Y. Zhang, T. Li, J. Kim, C.-Y. Chim, G. Galli, F. Wang, *Nano Lett.* **2010**, *10*, 1271; b) K. F. Mak, C. Lee, J. Hone, J. Shan, T. F. Heinz, *Phys. Rev. Lett.* **2010**, *105*, 136805; c) L. Britnell, R. M. Ribeiro, A. Eckmann, R. Jalil, B. D. Belle, A. Mishchenko, Y.-J. Kim, R. V. Gorbachev, T. Georgiou, S. V. Morozov, A. N. Grigorenko, A. K. Geim, C. Casiraghi, A. H. C. Neto, K. S. Novoselov, *Science* **2013**, *340*, 1311; d) A. M. Jones, H. Yu, N. J. Ghimire, S. Wu, G. Aivazian, J. S. Ross, B. Zhao, J. Yan, D. G. Mandrus, D. Xiao, W. Yao, X. Xu, *Nat. Nanotechnol.* **2013**, *8*, 634.

[3] a) K. S. Novoselov, A. Mishchenko, A. Carvalho, A. H. Castro Neto, *Science* **2016**, *353*, aac9439; b) A. K. Geim, I. V. Grigorieva, *Nature* **2013**, *499*, 419; c) D. Jariwala, T. J. Marks, M. C. Hersam, *Nat. Mater.* **2016**, *16*, 170.

[4] a) C.-H. Lee, G.-H. Lee, A. M. van der Zande, W. Chen, Y. Li, M. Han, X. Cui, G. Arefe, C. Nuckolls, T. F. Heinz, J. Guo, J. Hone, P. Kim, *Nat. Nanotechnol.* **2014**, *9*, 676; b) M.-Y. Li, Y. Shi, C.-C. Cheng, L.-S. Lu, Y.-C. Lin, H.-L. Tang, M.-L. Tsai, C.-W. Chu, K.-H. Wei, J.-H. He, W.-H. Chang, K. Suenaga, L.-J. Li, *Science* **2015**, *349*, 524; c) R. Cheng, D. Li, H. Zhou, C. Wang, A. Yin, S. Jiang, Y. Liu, Y. Chen, Y. Huang, X. Duan, *Nano Lett.* **2014**, *14*, 5590.

[5] S. Bertolazzi, J. Brivio, A. Kis, *ACS Nano* **2011**, *5*, 9703.

[6] a) M.-Y. Tsai, A. Tarasov, Z. R. Hesabi, H. Taghinejad, P. M. Campbell, C. A. Joiner, A. Adibi, E. M. Vogel, *ACS Appl. Mater. Interfaces* **2015**, *7*, 12850; b) J. Pu, Y. Yomogida, K.-K. Liu, L.-J. Li, Y. Iwasa, T. Takenobu, *Nano Lett.* **2012**, *12*, 4013; c) G.-H. Lee, Y.-J. Yu, X. Cui, N. Petrone, C.-H. Lee, M. S. Choi, D.-Y. Lee, C. Lee, W. J. Yoo, K. Watanabe, T. Taniguchi, C. Nuckolls, P. Kim, J. Hone, *ACS Nano* **2013**, *7*, 7931; d) W. G. Song, H.-J. Kwon, J. Park, J. Yeo, M. Kim, S. Park, S. Yun, K.-U. Kyung, C. P. Grigoropoulos, S. Kim, Y. K. Hong, *Adv. Funct. Mater.* **2016**, *26*, 2426.

[7] a) M. N. Blonsky, H. L. Zhuang, A. K. Singh, R. G. Hennig, *ACS Nano* **2015**, *9*, 9885; b) K.-A. N. Duerloo, M. T. Ong, E. J. Reed, *J. Phys. Chem. Lett.* **2012**, *3*, 2871; c) W. Wu, L. Wang, Y. Li, F. Zhang, L. Lin, S. Niu, D. Chenet, X. Zhang, Y. Hao, T. F. Heinz, J. Hone, Z. L. Wang, *Nature* **2014**, *514*, 470.

[8] H. Zhu, Y. Wang, J. Xiao, M. Liu, S. Xiong, Z. J. Wong, Z. Ye, Y. Ye, X. Yin, X. Zhang, *Nat. Nanotechnol.* **2014**, *10*, 151.

[9] a) X. Wen, W. Wu, C. Pan, Y. Hu, Q. Yang, Z. Lin Wang, *Nano Energy* **2015**, *14*, 276; b) Y. Liu, Y. Zhang, Q. Yang, S. Niu, Z. L. Wang, *Nano Energy* **2015**, *14*, 257; c) Z. L. Wang, *Nano Today* **2010**, *5*, 540; d) W. Wu, Z. L. Wang, *Nat. Rev. Mater.* **2016**, *1*, 16031; e) C. Pan,

L. Dong, G. Zhu, S. Niu, R. Yu, Q. Yang, Y. Liu, Z. L. Wang, *Nat. Photonics* **2013**, *7*, 752.

[10] a) P. Lin, X. Chen, X. Yan, Z. Zhang, H. Yuan, P. Li, Y. Zhao, Y. Zhang, *Nano Res.* **2014**, *7*, 860; b) P. Lin, X. Yan, F. Li, J. Du, J. Meng, Y. Zhang, *Adv. Mater. Interfaces* **2017**, *4*, 1600842; c) T. Liu, C. Jiang, X. Huang, C. Du, Z. Zhao, L. Jing, X. Li, S. Han, J. Sun, X. Pu, J. Zhai, W. Hu, *Nano Energy* **2017**, *39*, 53; d) H. F. Liu, W. Liu, S. J. Chua, D. Z. Chi, *Nano Energy* **2012**, *1*, 316; e) P. Lin, X. Yan, Z. Zhang, Y. Shen, Y. Zhao, Z. Bai, Y. Zhang, *ACS Appl. Mater. Interfaces* **2013**, *5*, 3671.

[11] a) W. J. Yu, Y. Liu, H. Zhou, A. Yin, Z. Li, Y. Huang, X. Duan, *Nat. Nanotechnol.* **2013**, *8*, 952; b) T. Roy, M. Tosun, X. Cao, H. Fang, D.-H. Lien, P. Zhao, Y.-Z. Chen, Y.-L. Chueh, J. Guo, A. Javey, *ACS Nano* **2015**, *9*, 2071; c) M. M. Furchi, A. Pospischil, F. Libisch, J. Burgdörfer, T. Mueller, *Nano Lett.* **2014**, *14*, 4785.

[12] W. Zhang, J.-K. Huang, C.-H. Chen, Y.-H. Chang, Y.-J. Cheng, L.-J. Li, *Adv. Mater.* **2013**, *25*, 3456.

[13] a) C. Lee, H. Yan, L. E. Brus, T. F. Heinz, J. Hone, S. Ryu, *ACS Nano* **2010**, *4*, 2695; b) H. Li, Q. Zhang, C. C. R. Yap, B. K. Tay, T. H. T. Edwin, A. Olivier, D. Baillargeat, *Adv. Funct. Mater.* **2012**, *22*, 1385.

[14] a) H.-V. Han, A.-Y. Lu, L.-S. Lu, J.-K. Huang, H. Li, C.-L. Hsu, Y.-C. Lin, M.-H. Chiu, K. Suenaga, C.-W. Chu, H.-C. Kuo, W.-H. Chang, L.-J. Li, Y. Shi, *ACS Nano* **2016**, *10*, 1454; b) S. Mouri, Y. Miyauchi, K. Matsuda, *Nano Lett.* **2013**, *13*, 5944; c) W. Zhou, X. Zou, S. Najmaei, Z. Liu, Y. Shi, J. Kong, J. Lou, P. M. Ajayan, B. I. Yakobson, J.-C. Idrobo, *Nano Lett.* **2013**, *13*, 2615; d) X. Zhang, Q. Liao, S. Liu, Z. Kang, Z. Zhang, J. Du, F. Li, S. Zhang, J. Xiao, B. Liu, Y. Ou, X. Liu, L. Gu, Y. Zhang, *Nat. Commun.* **2017**, *8*, 15881.

[15] M. Amani, D.-H. Lien, D. Kiriya, J. Xiao, A. Azcatl, J. Noh, S. R. Madhvapathy, R. Addou, S. Kc, M. Dubey, K. Cho, R. M. Wallace, S.-C. Lee, J.-H. He, J. W. Ager, X. Zhang, E. Yablonovitch, A. Javey, *Science* **2015**, *350*, 1065.

[16] L.-P. Feng, J. Su, Z.-T. Liu, *J. Alloys Compd.* **2014**, *613*, 122.

[17] a) K. F. Mak, K. He, C. Lee, G. H. Lee, J. Hone, T. F. Heinz, J. Shan, *Nat. Mater.* **2012**, *12*, 207; b) J. S. Ross, S. Wu, H. Yu, N. J. Ghimire, A. M. Jones, G. Aivazian, J. Yan, D. G. Mandrus, D. Xiao, W. Yao, X. Xu, *Nat. Commun.* **2013**, *4*, 1474.

[18] Z. Liu, M. Amani, S. Najmaei, Q. Xu, X. Zou, W. Zhou, T. Yu, C. Qiu, A. G. Birdwell, F. J. Crowne, R. Vajtai, B. I. Yakobson, Z. Xia, M. Dubey, P. M. Ajayan, J. Lou, *Nat. Commun.* **2014**, *5*, 5246.

[19] S. K. Kim, R. Bhatia, T.-H. Kim, D. Seol, J. H. Kim, H. Kim, W. Seung, Y. Kim, Y. H. Lee, S.-W. Kim, *Nano Energy* **2016**, *22*, 483.

[20] a) A. M. van der Zande, P. Y. Huang, D. A. Chenet, T. C. Berkelbach, Y. You, G.-H. Lee, T. F. Heinz, D. R. Reichman, D. A. Muller, J. C. Hone, *Nat. Mater.* **2013**, *12*, 554; b) V. Chikan, D. F. Kelley, *J. Phys. Chem. B* **2002**, *106*, 3794.

[21] a) W. Wu, L. Wang, R. Yu, Y. Liu, S.-H. Wei, J. Hone, Z. L. Wang, *Adv. Mater.* **2016**, *28*, 8463; b) G. Ho Ahn, M. Amani, H. Rasool, D.-H. Lien, J. P. Mastandrea, J. Ager, M. Dubey, D. C. Chrzan, A. M. Minor, A. Javey, *Nat. Commun.* **2017**, *8*, 608.

[22] M.-H. Chiu, C. Zhang, H.-W. Shiu, C.-P. Chuu, C.-H. Chen, C.-Y. S. Chang, C.-H. Chen, M.-Y. Chou, C.-K. Shih, L.-J. Li, *Nat. Commun.* **2015**, *6*, 7666.

[23] D. Q. Zheng, Z. Zhao, R. Huang, J. Nie, L. Li, Y. Zhang, *Nano Energy* **2017**, *32*, 448.

[24] A. Pezeshki, S. H. H. Shokouh, T. Nazari, K. Oh, S. Im, *Adv. Mater.* **2016**, *28*, 3216.

[25] a) P. Lin, Y. Gu, X. Yan, S. Lu, Z. Zhang, Y. Zhang, *Nano Res.* **2016**, *9*, 1091; b) C.-Y. Tsai, K. Gupta, C.-H. Wang, C.-P. Liu, *Nano Energy* **2017**, *34*, 367.